J Nanostruct 12(3): 697-710, Summer 2022

RESEARCH PAPER

Synthesis of Inverse Spinel Nickel Ferrite Like- Broccoli Nanoparticle and Thermodynamic Study of Photo-decolorization of Alkali Blue 4B dye

Ali Ameer Abd Zaid [1], *Luma M. Ahmed*[1]*, *and Rajaa K. Mohammad* [2]

[1] *Department of Chemistry, College of Science, University of Kerbala, 56001, Iraq*

[2] *Department of Physics, College of Science, University of Kerbala,56001, Iraq*

ARTICLE INFO

Article History:
Received 15 March 2022
Accepted 21 June 2022
Published 01 July 2022

Keywords:
Activation energy
Alkali blue 4B dye
Inverse spinel Nickel ferrite
Nickel ferrite
Non- ionic surfactant
Solvothermal method

ABSTRACT

Inverse spinel nickel ferrite ($NiFe_2O_4$ (or) $NiO.Fe_2O_3$) like- broccoli shape was manufactured as a brown nanoparticle. The $NiFe_2O_4$ preparation is done in the presence of the mixture of precursor salts in a ratio (2:1) of the iron ion with nickel ion prior to the presence of a nonpolar surfactant (hexamine). Hexamine acts as a capping agent before adding ammonia to solution; template and stabilizer via growth and storage of its powder. The solvothermal technique aided the precipitation route by using ethanol solvent at 180°C for 90 minutes to depress the defect in the prepared nanoparticle. The XRD data revealed that the $NiFe_2O_4$ peaks were wide and had a modest mean crystal size (20.13 nm). The broccoli-like $NiFe_2O_4$ nanoparticles with homogenous agglomerations were investigated using SEM- EDX analysis. The particle size is found to be 30.67 nm composing 100% of Ni, Fe, and O atoms. The - FT-IR analysis exhibited the positions of the tetrahedral site for (Fe^{3+}-O^{2-}) and octahedral site peaks for (Ni^{2+}- O^{2-}), and proved the type of $NiFe_2O_4$ is an inverse spinal structure. The $NiFe_2O_4$ has been owned as an excellent optical property with a small indirect band gap value (2.05 eV). Following this fact, this spinal can be used as a photocatalyst. The best photo-decolorization of this dye took place at pH 7 as a pseudo-first order with efficiency (98 %). This photoreaction is fast, endothermic and non-spontaneous. Negative entropy value refers to the products in this dye decolorization being more regular than the reactant (dye) structure.

How to cite this article
Abd Zaid A A, Ahmed L M, Mohammad R K. Synthesis of Inverse Spinel Nickel Ferrite Like- Broccoli Nanoparticle and Thermodynamic Study of Photo-decolorization of Alkali Blue 4B dye. J Nanostruct, 2022; 12(3):697-710. DOI: 10.22052/JNS.2022.03.022

INTRODUCTION

The discharge of untreated wastewater containing dyes directly into natural water bodies is detrimental to the photosynthetic activity of aquatic ecosystems. Due to the presence of metals and aromatic compounds, it causes mutagenic or teratogenic effects on aquatic creatures including fish. In addition, the presence of dyes in the environment has minor to severe hazardous impacts on human health, such as carcinogenic, mutagenic, allergy, dermatitis, and renal disease consequences. It has been found that chromium-based dyes are often structurally complicated and carcinogenic to human health[1].There are several diverse families of dyes, like: anthraquinone, azo, triphenylmethane, indigo, triarylmethane have

* *Corresponding Author Email: luma.ahmed@uokerbala.edu.iq*

recently been studied and proved they are optically nonlinear under continuous and pulsed wave regimes. Triarylmethane is an important kind of synthetic dye and is widely used in antimicrobial, antifungal, and antitubercular activities[2]. Triarylmethane dyes are widely utilized in the textile and dying industries due to their vivid color and inexpensive cost. The primary structure of triarylmethane dyes is obtained from the existence of monomethine with three terminal aryl groups as chromophores and functionalization by hydroxyl, amino, or dimethyl amino auxochromic groups[3]. One of type Triarylmethane dye is Akali blue 4B (acid blue 110)[4]. Due to the toxicity and hazard of dyes, there are a variety of ways to eliminate them in wastewater adsorption, photocatalysis, photodegradation, membrane filtration, oxidation, and irradiation[5]. In addition, nanoparticles of metal are used to decolorize colored effluent. The size and form of nanoparticles have a significant impact on decolorization and may be manipulated via a variety of physical and chemical methods. These particles have a propensity to agglomerate, reducing their activity[6].Spinel nanocrystals are thought to be two of the most important inorganic nanomaterial's because of their electronic, optical, electrical, magnetic, and catalytic properties. A and B make up the AB_2O_4 structure of spinel, which represented the tetrahedral and the octahedral binary cation and trinity cation binding sites, respectively. The O stands for the oxygen anion location. The spinel ferrite metal is a widespread and vital exam for spinel materials. The general molecular formula applies is MFe_2O_4 (M = Ni, Zn, Mn, Co, or Mg) and has a face-centered-cubic (fcc) tight packing structure. The spinel ferrites compounds such as zinc ferrite, manganese ferrite, cobalt ferrite, and nickel ferrite. The metal ferrites have been widely investigated because of their inverse, normal, and mixed-use buildings form distinct architectural forms. The spinel crystal formations have a high electromagnetic conductivity, mechanical hardness, low coercively, high performance, outstanding chemical stability, and mild saturation magnetization. As a result, it is a strong candidate for the application, high-frequency soft magnets and low-loss materials[7]. Ni ferrite ($NiFe_2O_4$) is one of the inverse spiels. Half of the iron ions in Ni ferrite are in the tetrahedral sites (A-site), and the other half is in the oxygen sites. Ni ions are found in octahedral positions (B-site)[8]. The $NiFe_2O_4$ is one of the most significant spinel ferrites researched. It is an n-type semiconductor according to its stoichiometry. Depending on the particle size and shape, it shows a variety of magnetic characteristics, including paramagnetic, super paramagnetic, and ferromagnetic behavior. Furthermore, when its size is lowered to nanometers, it shows remarkable physical and chemical properties[9]. At room temperature, the UV–Vis diffuse spectra explain that the $NiFe_2O_4$ is an indirect band gap material with various sintering temperatures from 1.78 to 2.72 eV [10,11]. Nickel ferrite is one of the most significant ferrous spinel alloys with a super-magnetic nature and a wide range of applications, such as gas sensors, liquid magnetism, catalysts, magnetic storage systems, photomagnetic materials, imaging devices, microwaves, magnetic cooling, as a microwave absorber, magnetic resonance, and, in biomedicine, for example, local drug delivery[12,13]. The magnetic properties of nanoparticles used in a variety of sectors are mostly determined by their size, shape, purity, and magnetic stability (e.g., blocked or unblocked state at a particular operating temperature). These particles should exist in a single domain state with a pure phase, high coercivity, and modest magnetism. Based on from an application standpoint, the super paramagnetic blocking temperature of the nanoparticles utilized for recording is rather low. For reliable data recording in these devices, their temperatures must be far above room temperature. In medical applications In place of traditional drug delivery systems, magnetic nanoparticles are utilized as drug carriers inside the body. Possibly ineffective delivery systems[9]. In the last few years, many physical and chemical methods have been used to synthesize nano-size ferrites. Since structural, magnetic and electrical properties of ferrites depends on their composition and microstructure and hence are strongly dependent on the synthesis method and synthesis conditions, some of these methods are Co-precipitation, Hydrothermal, Sol-gel, Thermal decomposition Method, Solvothermal Method, Sonochemical, Microwave-assisted Method, Microemulsion Method, Electrochemical, Mechanical milling Method [14]. This work focuses on the preparation and characterization and application of inverse spinal $NiFe_2O_4$ nanoparticle by precipitation process in the presence of the non- ionic surfactant (hexamine) and assisted by a solvothermal route. The XRD, SEM-EDX, FT-IR

and Bg were studied of the as-prepped $NiFe_2O_4$ nanoparticle. In addition, the effect of pH and the thermodynamics function were estimated for the photo-decolorization of alkali blue 4B dye.

MATERIALS AND METHODS

Chemicals

The powdered ore of Ferric nitrate $Fe(NO_3)_3.9H_2O$ and Nickel nitrate $Ni(NO_3)_2.9H_2O$ were purchased by sigma cheml co. USA. Ammonia solution (25 percent) was supplied from Merck. Absolute ethanol (C_2H_5OH) and Hexamethylenetetramine (methenamine or hexamine) that includes a cage-like structure were outfitted from BDH and Interchimiques SA, respectively. The dye alkali blue 4B ($C_{32}H_{28}N_3NaO_4S$) was purchased by Merck. This dye is acidic type, molar mass = 573.64 g/mol, and the Structure as Fig. 1.

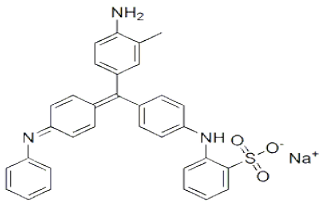

Fig. 1. The Structure of a dye alkali blue 4B.

Procedure

This procedure was monitored using two mixed solutions in a stoichiometric ratio (2:1) that was modified from the reference [15]. Based on Fig. 2, solution 1 contained 0.2 M of Ferric nitrate $Fe(NO_3)_3.9H_2O$ in 50 mL D.W under ultrasonic waves for 10 min. Solution 2 obvious contained 0.1 M of Nickel nitrate $Ni(NO_3)_3.6H_2O$ in 50 mL D.W under ultrasonic waves for 10 min. Inside the ultrasonic bath, solution 2 was added step by step to solution 1 and mixed for 10 min. The final pH of this produced solution was measured to be about 3. An exact 0.5 g of hexamine (non-ionic surfactant) was added to solution as a capping agent, template and stabilizer, with continuous mixed using a magnetic stirrer at 60 °C for 10 min. After that, the pH of solution must be fixed using conc. ammonia solution that drop-wise added until raised to about 9.5 to 10 under stirring continued for 30 min at 60 °C. The brown solution was produced; this solution was filtered and washed with D.W and ethanol. In order to improve the properties of the brown precipitate, it was dispersive in 50 mL of Ethanol, then transported to a Teflon cup sealed in an autoclave hydrothermal instrument and heated in an oven at 180 °C for 90 min. After cooling the steles steal autoclave in air, the suspension solution was filtered and washed by 50 mL D.W then 30 mL of ethanol to ensure all the amounts of negative ions of precursor salts and humidity are removed. This precipitate was thrown to dry using silica gel inside a desiccator for overnight.

The chemical reactions of producing the inverse spinel $NiFe_2O_4$ were suggested using the reactions 1-2.

The suggested mechanism of using non –polar surfactant during the preparation of nickel ferrite can be depicted in Fig. 3. The step of addition of surfactant during precipitation method is vital to be capping agent and template in the same time that attitude to prevent formation of metal hydroxide, and produce homogenously growth for $NiFe_2O_4$ nanoparticle, respectively. Moreover, the non-polar surfactant is also important to ensure the stabilization of formed nano-compound during the storage process.

Application of the Spinel $NiFe_2O_4$ used to decolorize alkali blue 4B dye solution

A homemade photo reactor was used to carry out the photoreaction in Fig. 4. This photoreactor is equipped with a 400-watt UV light that is put inside a wooden box as a reactor's body to prevent the UV-A light risk. The light source was positioned directly above the Pyrex glass beaker (500 mL) to ensure a good focusing of it. Moreover, a magnetic stirrer, a Teflon bar, and used two different fans to fix and eliminate the generated heat from the lamp[17–20].

At a temperature 25 °C, exactly 0.025 g of spinel $NiFe_2O_4$ was added to 25 ppm from alkali blue 4B

$$Ni(NO_3)_2.6H_2O + 2Fe(NO_3)_3.9H_2O + 8NH_4OH \xrightarrow{surfactant} Ni(OH)_2.Fe_2(OH)_6 + 8NH_4NO_3 + 24H_2O \quad (1)$$

$$Ni(OH)_2.Fe_2(OH)_6 \rightarrow NiO.Fe_2O_3 \text{ or } NiFe_2O_4 + 4H_2O \quad (2)$$

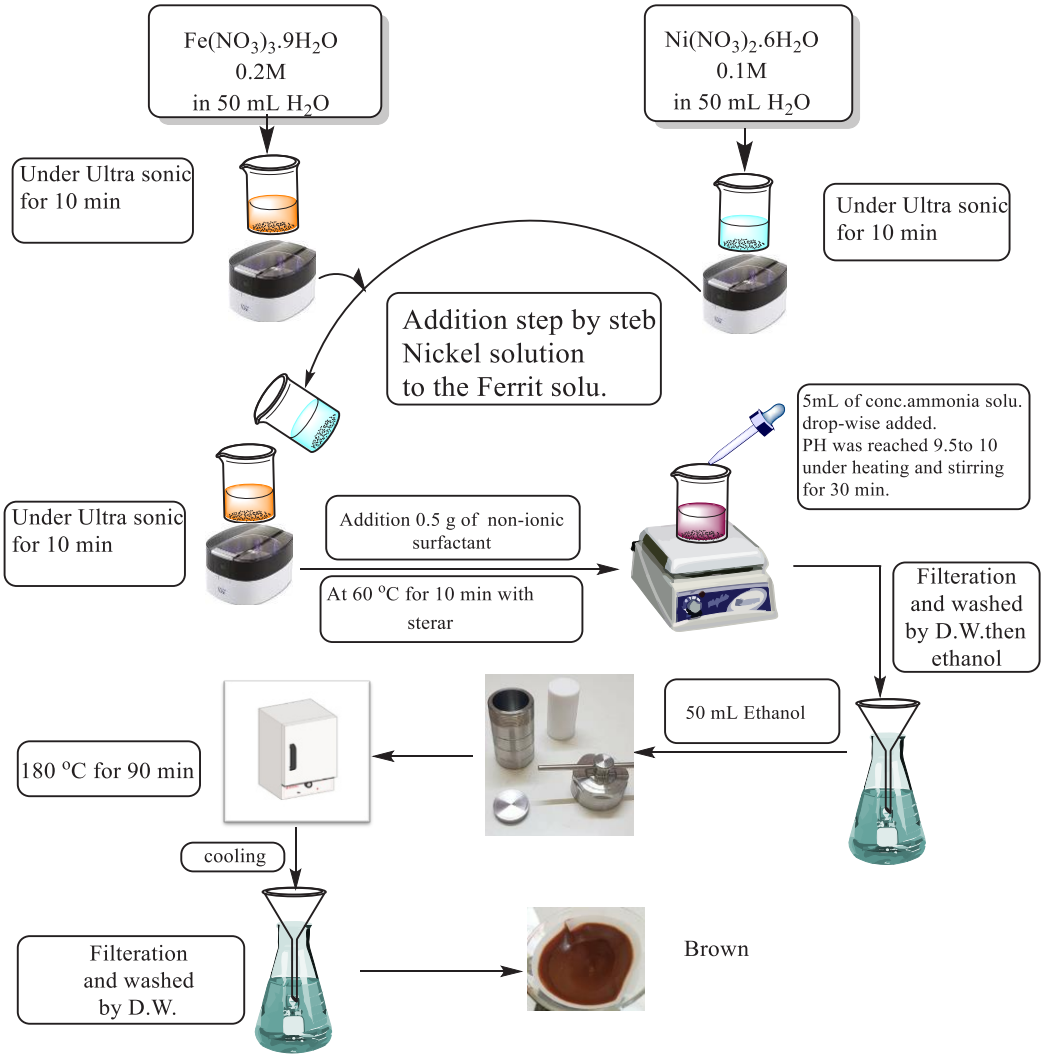

Fig. 2. The schematic diagram of preparation steps of Nickel ferrite nanoparticle.

dye solution at pH 2.5. Without irradiation, the suspension solution was magnetically agitated for 15 minutes to allow for the establishment of an equilibrium adsorption condition[21-23]. Following the adsorption stage, the suspension was exposed to UV light, and about 5 mL of aliquots were collected at intervals time started from 5 minutes until 35 minutes. The collected suspensions were centrifuged twice at 6000 rpm for 20 minutes. The absorbance of the resulting filters was measured at 593 nm using a UV-Vis spectrophotometer (FAITHFUL model 721). The apparent rate constant for the first order equation [24-26] and the % efficiency of dye photo-decolourization [27-29] were calculated using equations 1 and 2.

$$\ln\left[\frac{C_0}{C_t}\right] = K_{app} \times t \quad (1)$$

$$E\% = \left[\frac{C_0 - C_t}{C_0}\right] \times 100 \quad (2)$$

RESULT AND DISCUSSION

Structure properties

The XRD analysis of the structure of prepared spinal $NiFe_2O_4$ with ranging from 0° to 80° using a Lab X XRD 6000-Shimadzu is represented in Fig. 5. The XRD data of $NiFe_3O_4$ synthesized powder exhibited the three essential not sharp peaks,

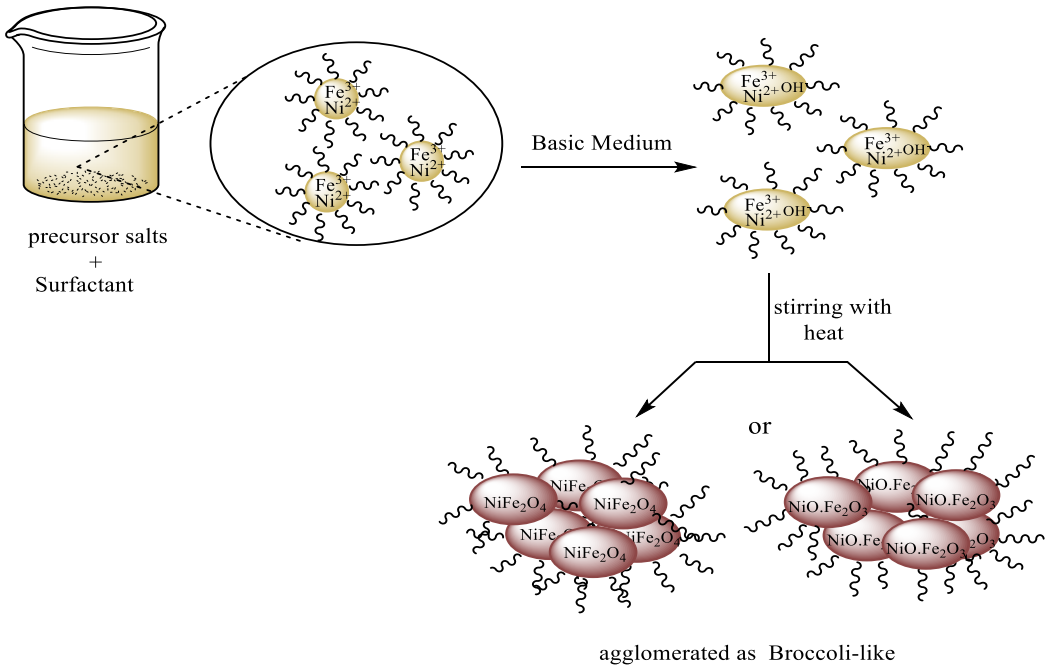

Fig. 3. The suggested mechanism for role using of non-polar surfactant during preparation Nickel ferrite nanopartical. (Modified from reference16).

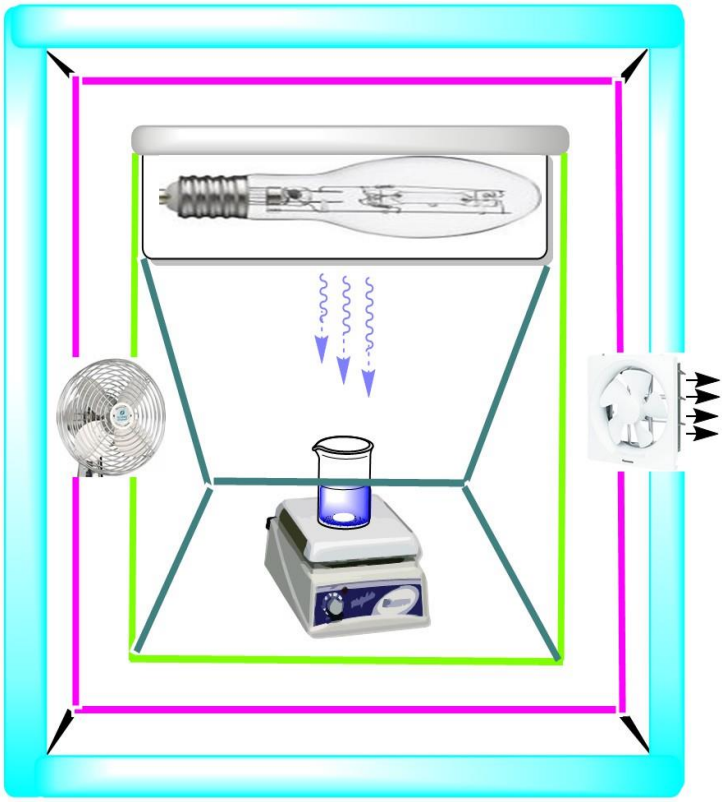

Fig. 4. Diagrammatic representation of a Homemade Photocatalytic Reactor Unit.

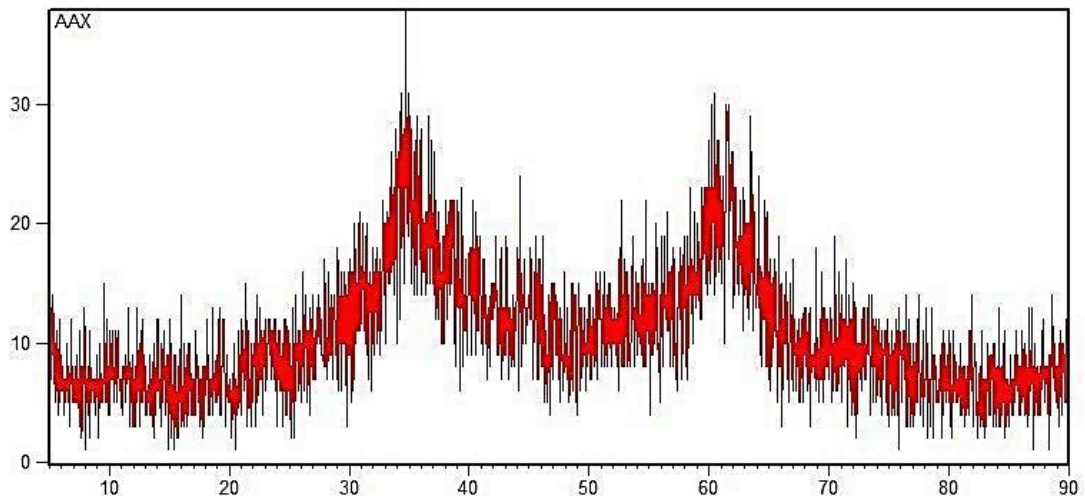

Fig. 5. XRD pattern of spinel $NiFe_2O_4$ nanoparticle.

with diffraction patterns at 2θ = 35.77°, 43.51°, 63.04° that correspond to the planes of (311), (400), and (440), respectively (Card No.: 00-003-0875). In contrast to diffraction patterns of perfect crystals[30, 31]. These results are in agreement with another study for preparing the $NiFe_2O_4$ nanoparticle before calcinated it [15].

The mean crystallite size (L) in nm was calculated for spinal $NiFe_2O_4$ powder using the Scherer's equation(3)[32-37], and found to be 20.13 nm**.** It seems that the produced size of the prepared spinal $NiFe_2O_4$ powder is nanomaterial (less 100 nm)[38,39]. This result enhanced the good bending between Ni^{2+} and Fe^{3+} by the metallic bonds in crystal lattices of spinal $NiFe_2O_4$ nanoparticle, which due to the nearly ionic radii that equal to 0.59 Å and 0.609 Å, respectively[40].

$$L = \frac{K.\lambda}{\beta.Cos\theta} \quad (3)$$

Where k, denotes the shape constant, λ is Cu's wavelength used as a source of x-ray, 2θ is a Bragg

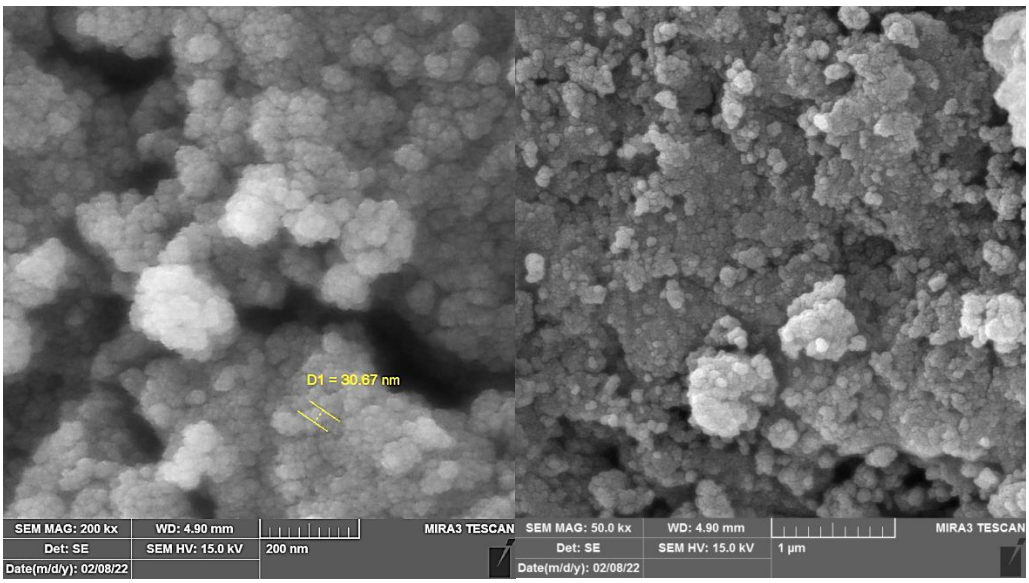

Fig. 6. SEM images of the inverse spinel $NiFe_2O_4$ nanoparticle.

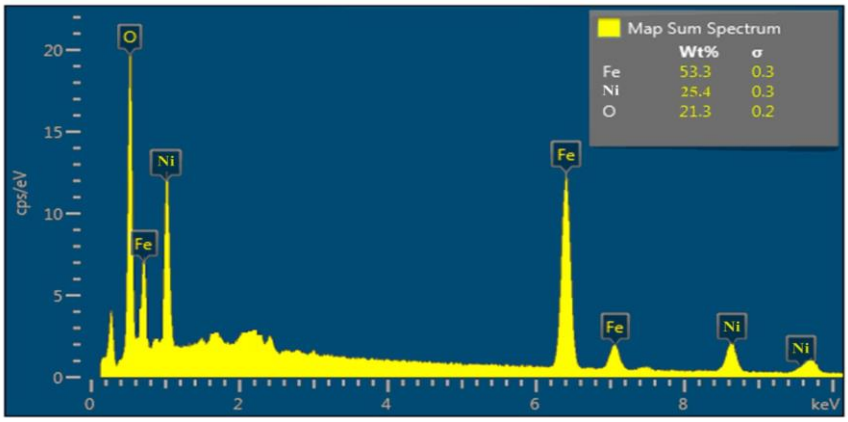

Fig. 7. EDX spectrum of the inverse spinel $NiFe_2O_4$ nanoparticle.

diffraction angle, and (FWHM) is meaning a full width at half maximum intensity.

Morphology of studied photo catalyst surfaces
SEM analysis

It was used to determine the morphology of the sample surface using (FESEM FEI Nova Nano SEM 450). The SEM images of spinel Nickel Ferrite surfaces display in Fig. 6. The SEM analysis reveals that the sample shows a compressed order of homogenous nanoparticles with an almost spherical shape that agglomerated to form a like-broccoli nanoparticle shape. Most particles are assembled, hence, the particle size is more valuable than the mean crystal size[41, 42] and equal to 30.67 nm. This behavior may be attributed to the small dimensions of nanoparticles and has a high density [15]. The $NiFe_2O_4$ nanoparticle pieces of evidence it is a polycrystalline structure.

EDX analysis

It was used to validate the sample's components. As seen in Fig. 7, the nickel ferrite illustrates the Ni, Fe and O elements uniformity distribution in

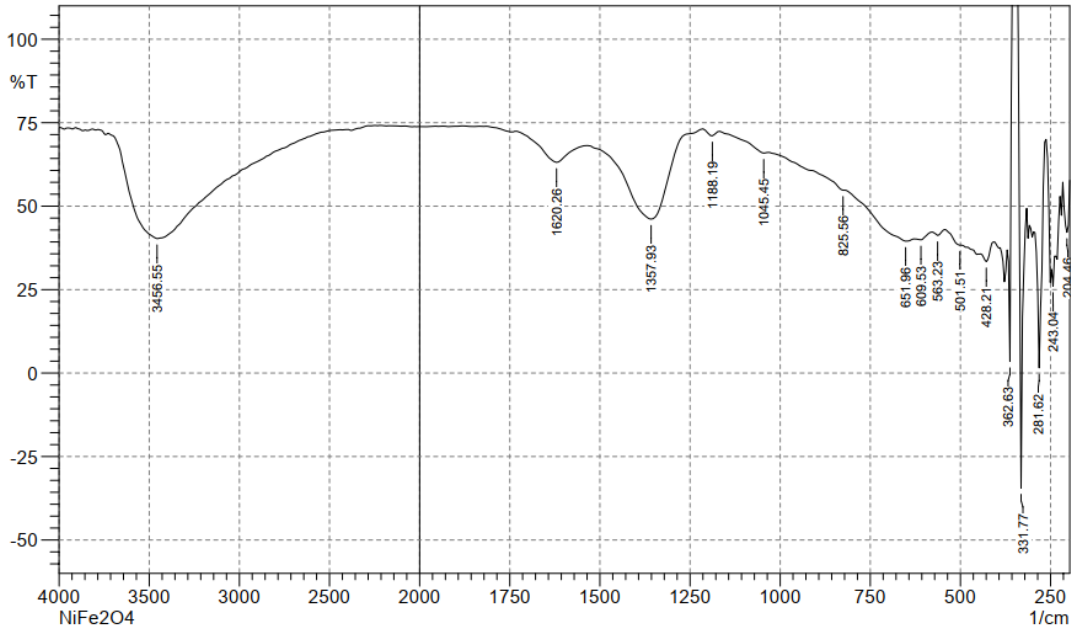

Fig. 8. FTIR spectrum images of the inverse spinel $NiFe_2O_4$ nanoparticle.

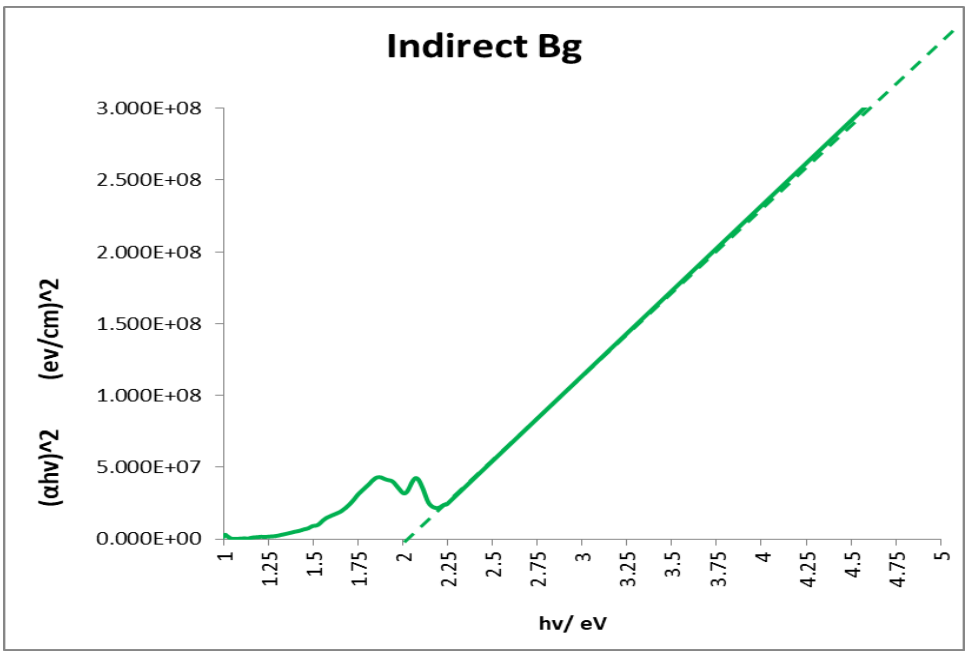

Fig. 9.The band gap of prepared the inverse spinel $NiFe_2O_4$ nanoparticle.

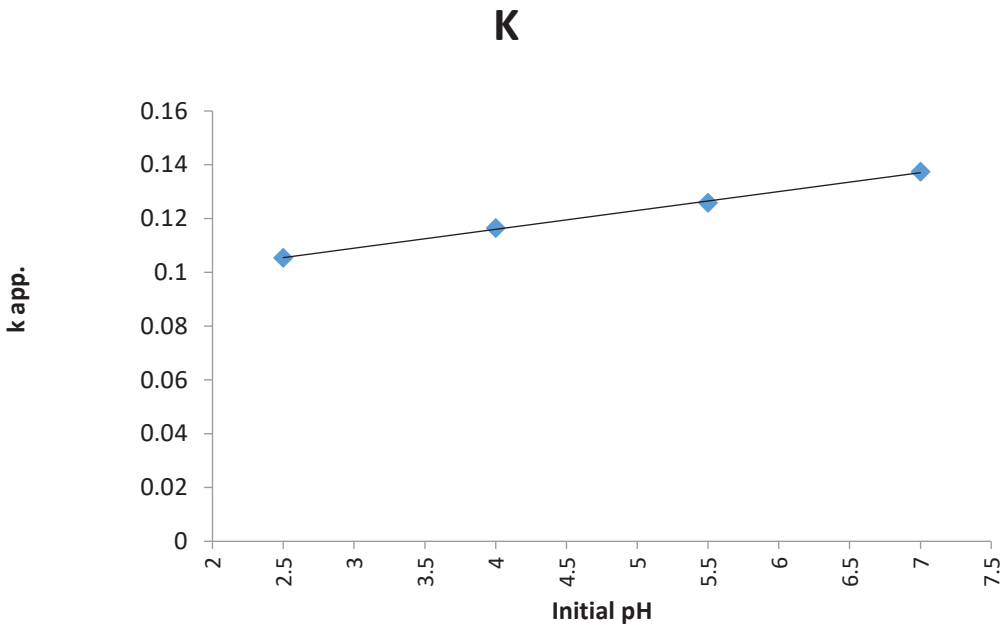

Fig. 10. Effect of Initial pH:(first order rate constant at varying initial pH of Alkali blue 4B dye with semiconductor inverse spinel $NiFe_2O_4$ nanoparticle on photodecolorization)

the polycrystalline layer without any impurities. Moreover, the wt % of Fe is found to be double than the wt % of Ni, this is good agreement with the stoichiometry preparation ratio (2:1) that is used in the preparation procedure[15], and reported in references[43,44].

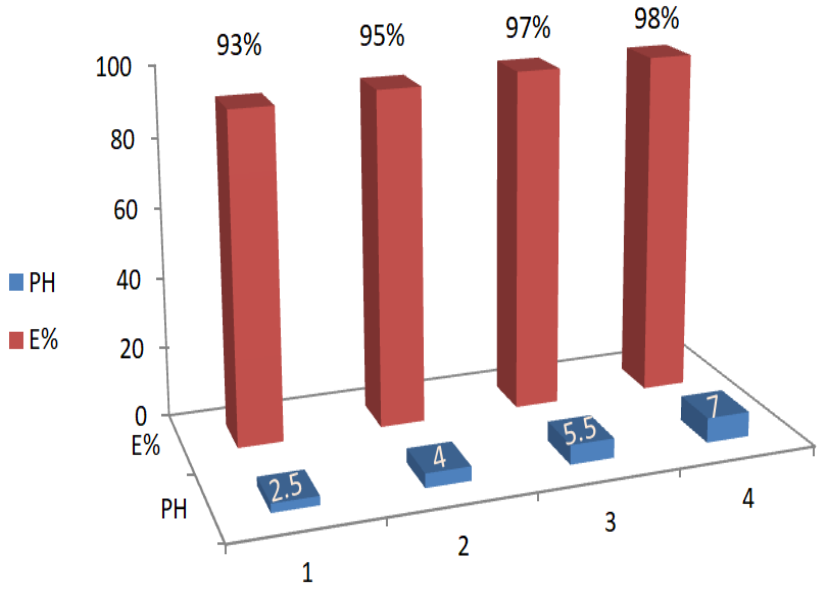

Fig. 11. The relationship between (PDE %) V.S initial pH of studied dye.

Optical Properties

FTIR Analysis

The location of the ions in the crystal structure and their modes of vibration are revealed by FTIR spectra, revealing the various arrangement locations on the structural characteristics of composites. In this study, the FTIR spectra of the produced sample were analyzed using Shimadzu 8400S Japan equipment throughout the range of 250–4000 cm^{-1} using a CsI disk.

As seen in Fig. 8 the FT-IR spectra of all spinels, and especially ferrites includes two primary wide metal oxygen bands are seen below about 600 cm^{-1} beyond tetrahedral and octahedral sites[45]. The tetrahedral is short bond therefore it lies in a high frequency vibration site. Nickel

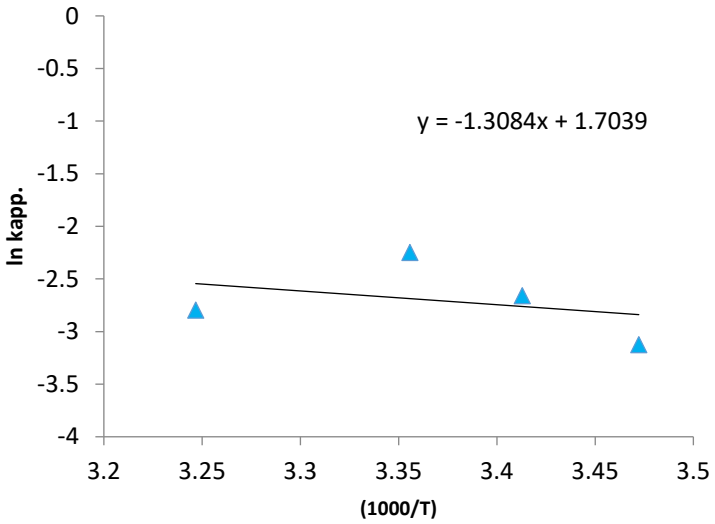

Fig. 12. The Arrhenius equation plot for photoreaction in the presence the inverse spinel $NiFe_2O_4$ nanoparticle.

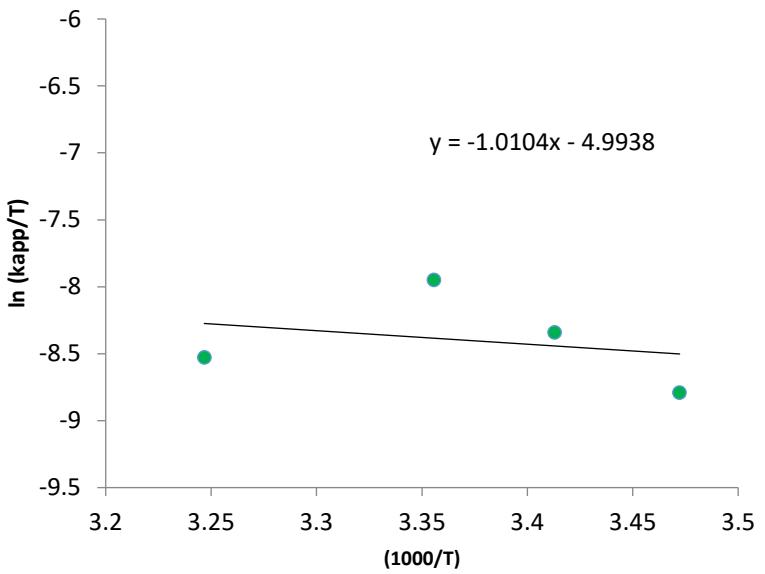

Fig. 13. The Eyring-Polanyi equation plot for photoreaction in the presence the inverse spinel $NiFe_2O_4$ nanoparticle

ferrite is having an inverse spinel structure group, therefore, the highest-frequency band, seen at v1 = (563.23-651.93) cm^{-1}, is attributed to tetrahedral site vibrations of $(Fe\text{-}O)_{tetra}$, while at the lowest-frequency band, seen at v2= (362.63-428.21) cm^{-1}, is attributed to octahedral site vibrations of $(Ni\text{-}O)_{octa.}$.These results are in good agreement with the reported for similar Metal ferrite [45-48]. The bands at 3456.55 cm^{-1} and 1620 cm^{-1} correspond to the manner of stretching mode of H_2O and OH molecules as a broad band and bending mode of H_2O molecules, respectively [45,47]. The use a hexamine as a non- polar surfactant as a capping agent and stabilizer for Ni ferrite leads to appear the bands at 1367 cm^{-1} and the band at 1118 cm^{-1} may be beyond the C-H bending vibrations and C-N stretching vibration [49].

The band gaps energy

The optical energy bandgaps (Eg) value in eV revealed information about the ability of this material to investigate as a photocatalyst[50,51]. The bandgap can be determined for all photocatalyst samples using the Tauc equation[52,53] equation 4, which is based on the absorption coefficient (α) in equation 5 that depended on the thickness (t) and the absorbance (A).

$$\alpha h\nu = k(h\nu - Eg)^m \quad (4)$$

$$\alpha = (2.3026\ A)/t \quad (5)$$

Where h, , *k*, and m are Plank's constant the light, frequency, optical constant and constant value equal to ½ or 2 for direct and indirect transitions, respectively.

Equation 4 is plotted in Fig. 9, and demonstrated that the band gap of as- prepared inverse spinel $NiFe_2O_4$ nanoparticle is an indirect band gap [54,55], and equal to 2.05 eV.

Photo-decolorization of Alkali blue 4B dye

The effectiveness of the prepared inverse spinel $NiFe_2O_4$ nanoparticle was estimated, based on the value of the band gap, so, this spinel was applied in a photochromic decolorization of Alkali blue 4B dye.

The influencing of initial pH of dye solution on the photo-decolorization process

This manner was done with the pH ranging equal to 2.5, 4, 5.5, and 7. The initial pH of this dye was found to be 2.5. In Figs. 10 and 11, it was observed that the percentage of dye photo-decolorization and photo-decolorization rate increase with the increasing pH ranging from 2.5 to 7. That is due to the increase in an attractive force between the dye molecule and catalyst surface because of dye is having acidic nature. Moreover, the percentage of

Table 1.The Calculated activation energy and thermodynamic functions for decolonization reaction of Alkali blue 4B dye with prepared the normal spinel $NiFe_2O_4$ nanoparticle.

Samples	E_a /kJ mol^{-1}	$\Delta H^{\#}$ /kJ mol^{-1}	$\Delta S^{\#}$ /kJ mol^{-1} K^{-1}	$\Delta G^{\#}$ /kJ mol^{-1}
$NiFe_2O_4$	10.878	8.400	-0.240	79.920

hydroxyl radicals is also increased in the solution , these causes lead to enhance the photocatalytic activity of the decolorization process [56,57].The pH value was not performed with an increase of more than 7 that attitude to the change in the color of the dye solution, which referred to the change in dye structure.

The influencing of temperature on the photo-decolorization of dye

This effect was performed at range of temperatures (15, 20, 25, 35) °C using 25 ppm of dye with 0.01 g of inverse spinel nickel ferrite. It was found that the best temperature for the reaction is 25 °C. The Arrhenius equation plot (equation 6)[58,59] and the Ering-Pollani equation plot (equation 7)[[60-63] were done in Fig. 12 and Fig. 13, to find the activation energy (E_a), enthalpy ($\Delta H^{\#}$)and entropy ($\Delta S^{\#}$), respectively. Where: k_B is Boltzman constant (1.380649 × 10^{-23} m^2 kg s^{-2} K^{-1}) and h is Planck constant (6.626x10^{-34} Js), A is frequency factor, R is gas constant (8.314 J. mol^{-1}. K^{1-}).

$$ln\ k_{app} = \frac{-E_a}{RT} + ln\ A \quad (6)$$

$$ln(\frac{k_{app}}{T}) = \frac{-\Delta H^{\#}}{RT} + \left(ln(\frac{k_B}{h}) + \frac{\Delta S^{\#}}{R}\right) \quad (7)$$

The Gibbs energy (equation 8) was calculated depending on the values of $\Delta S^{\#}$ and $\Delta H^{\#}$ [64,56].

$$\Delta G^{\#} = \Delta H^{\#} - T\Delta S^{\#} \quad (8)$$

The calculated activation energy and thermodynamic functions were listed in Table 1. From the results, it was found that the photoreaction is endothermic, non-spontaneous and less random. These results are in agreement with the reported references [64-66]. The negative value of entropy (-0.240 kJ mol^{-1}) confirms that the transition state generated is low structural freedom compared to the reactant (dye molecule) through the decolonization process of this dye, which enhanced the real of the decolorization process is irreversible [57, 59]. The activation energy was a small value and equal to10.878 kJ mol $^{-1}$ that can be beyond the diffusion process in this photoreaction is controlled when its value less than 29 kJ mol^{-1}[57]. Also, the reaction on the spinel surface can happen in multiple chain steps, one is a fast step that appears when the bond on the octahedral Ni-O site is formed, and another is a slow due to form the bond on the tetrahedral Fe-O site, which needed to high energy to bind.

CONCLUSION

The vital results of this paper may be included:

1- The inverse spinel $NiFe_2O_4$ as nanoparticles like- broccoli was successfully prepared using the precipitation method that assisted with a hydrothermal method.

2- The non-polar surfactant (hexamine) was used in the preparation of inverse spinel $NiFe_2O_4$ and acts as a template, capping agent and stabilizer.

3- Using XRD analysis and SEM-EDX analysis, the inverse spinel $NiFe_2O_4$ nanoparticles are confirmed.

4- According to FT-IR spectrum, the positions of the octahedral Ni-O site and the tetrahedral Fe-O site was determined, and proved the inverse spinel $NiFe_2O_4$ nanoparticle were formed.

5- The bandgap of the inverse spinel $NiFe_2O_4$ nanoparticle was found to be indirect type.

6- The photoactivity in using the inverse spinel nanoparticle $NiFe_2O_4$ nanoparticles with alkali blue 4B dye depended on pH of solution and the best result can occurred in a neutral medium.

7- The photoreaction is a fast and obeyed pseudo-first order kinetic with low activation energy.

8- The low absolute values of Ea, $\Delta H^{\#}$, and $\Delta S^{\#}$ for the reaction estimated the prepared catalyst is having high catalytic activity to generate electron-hole pairs that lead to hydroxyl radical in aqueous solution.

ACKNOWLEDGMENTS

The authors would like to thank everyone who helped with this manuscript in the University of Kerbala's faculty of science- department of

chemistry and department of physics.

CONFLICT OF INTEREST

The authors declare that there is no conflict of interests regarding the publication of this manuscript.

REFERENCE

1. Dutta S, Gupta B, srivastava sK, Gupta AK. Recent advances on the removal of dyes from wastewater using various adsorbents: A critical review. Materials Advances. 2021.
2. Jeyaram S. Intermolecular charge transfer in donor–acceptor substituted triarylmethane dye for NLO and optical limiting applications. Journal of Materials Science: Materials in Electronics. 2021;32(7):9368-9376.
3. Sakti SCW, Laily RN, Aliyah S, Indrasari N, Fahmi MZ, Lee HV, et al. Re-collectable and recyclable epichlorohydrin-crosslinked humic acid with spinel cobalt ferrite core for simple magnetic removal of cationic triarylmethane dyes in polluted water. Journal of Environmental Chemical Engineering. 2020;8(4):104004.
4. Sessa C, Weiss R, Niessner R, Ivleva NP, Stege H. Towards a Surface Enhanced Raman Scattering (SERS) spectra database for synthetic organic colourants in cultural heritage. The effect of using different metal substrates on the spectra. Microchem J. 2018;138:209-225.
5. Efficient Removal of Dye from Wastewater without Selectivity Using Activated Carbon-Juncus effusus Porous Fibril Composites. American Chemical Society (ACS).
6. Kale RD, Kane PB. Colour removal using nanoparticles. Textiles and Clothing Sustainability. 2016;2(1).
7. Goodarz Naseri M, Saion EB, Kamali A. An Overview on Nanocrystalline $ZnFe_2O_4$, $MnFe_2O_4$, and $CoFe_2O_4$ Synthesized by a Thermal Treatment Method. ISRN Nanotechnology. 2012;2012:1-11.
8. Hajihashemi H, Kameli P, Salamati H. The Effect of EDTA on the Synthesis of Ni Ferrite Nanoparticles. Journal of Superconductivity and Novel Magnetism. 2012;25(7):2357-2363.
9. Khairy M, Gouda ME. Electrical and optical properties of nickel ferrite/polyaniline nanocomposite. Journal of Advanced Research. 2015;6(4):555-562.
10. Tong S-K, Chi P-W, Kung S-H, Wei D-H. Tuning bandgap and surface wettability of NiFe2O4 driven by phase transition. Sci Rep. 2018;8(1).
11. Kavas H, Kasapoğlu N, Baykal A, Köseoğlu Y. Characterization of NiFe2O4 nanoparticles synthesized by various methods. Chemical Papers. 2009;63(4).
12. Gupta N, Jain P, Rana R, Shrivastava S. Current Development in Synthesis and Characterization of Nickel Ferrite Nanoparticle. Materials Today: Proceedings. 2017;4(2):342-349.
13. Tatarchuk T, Bououdina M, Judith Vijaya J, John Kennedy L. Spinel Ferrite Nanoparticles: Synthesis, Crystal Structure, Properties, and Perspective Applications. Springer Proceedings in Physics: Springer International Publishing; 2017. p. 305-325.
14. Ahmad N, Alam M, Ansari AA, Alrayes BF, Ahmed M, Alotaibi MA. Nickel Ferrite Nanomaterials: Synthesis, Characterization and Properties. Nanoscience and Nanotechnology Letters. 2017;9(11):1688-1695.
15. Salvador M, Gutiérrez G, Noriega S, Moyano A, Blanco-López MC, Matos M. Microemulsion Synthesis of Superparamagnetic Nanoparticles for Bioapplications. Int J Mol Sci. 2021;22(1):427.
16. Ahmed L, S. Fadhil E, F. Mohammed A. Effect of silver doping on structural and photocatalytic circumstances of ZnO nanoparticles. Iraqi Journal of Nanotechnology. 2020(1):13-20.
17. Jaafar MT, Ahmed LM. Reduced the toxicity of acid black (nigrosine) dye by removal and photocatalytic activity of TiO_2 and studying the effect of pH, temperatue, and the oxidant agents. INTERNATIONAL CONFERENCE OF NUMERICAL ANALYSIS AND APPLIED MATHEMATICS ICNAAM 2019: AIP Publishing; 2020.
18. Hussain ZA, Fakhri FH, Alesary HF, Ahmed LM. ZnO Based Material as Photocatalyst for Treating the Textile Anthraquinone Derivative Dye (Dispersive Blue 26 Dye): Removal and Photocatalytic Treatment. Journal of Physics: Conference Series. 2020;1664(1):012064.
19. Alattar RA, Hassan ZM, Abass SK, Ahmad LM. Synthesis, characterization and study the photodecolorization of Schiff base Fe(III) complex in ZnO/Uv-A light system. INTERNATIONAL CONFERENCE OF NUMERICAL ANALYSIS AND APPLIED MATHEMATICS ICNAAM 2019: AIP Publishing; 2020.
20. Karam F, Saeed N, Al Yasasri A, Ahmed L, Saleh H. Kinetic Study for Reduced the Toxicity of Textile Dyes (Reactive yellow 14 dye and Reactive green dye) Using UV-A light/ZnO System. Egyptian Journal of Chemistry. 2020;0(0):0-0.
21. Alattar R, Saleh H, Al-Hilifi J, Ahmed L. Influence the addition of Fe2+ and H_2O_2 on removal and decolorization of textile dye (dispersive yellow 42 dye). Egyptian Journal of Chemistry. 2020;0(0):0-0.
22. Jawad TM, R. Al-Lami M, Hasan A, Al-Hilifi J, Mohammad R, Ahmed L. Synergistic Effect of dark and photoreactions on the removal and photo-decolorization of azo carmosine dye (E122) as food dye using Rutile- TiO_2 suspension. Egyptian Journal of Chemistry. 2021;0(0):0-0.
23. Li T, Wang T, Qu G, Liang D, Hu S. Synthesis and photocatalytic performance of reduced graphene oxide–TiO_2 nanocomposites for orange II degradation under UV light irradiation. Environmental Science and Pollution Research. 2017;24(13):12416-12425.
24. Ahmad I, Sheraz MA, Ahmed S, Kazi SH, Mirza T, Aminuddin M. Stabilizing effect of citrate buffer on the photolysis of riboflavin in aqueous solution. Results in Pharma Sciences. 2011;1(1):11-15.
25. Abass SK, Al-Hilfi JA, Abbas SK, Ahmed LM. Preparation, Characterization and Study of the Photodecolorization of Mixed-Ligand Binuclear Co(II) Complex of Schiff Base by ZnO. Indonesian Journal of Chemistry. 2020;20(2):404.
26. Hussein ZA, Abbas SK, Ahmed LM. UV-A activated ZrO_2 via photodecolorization of methyl green dye. IOP Conference Series: Materials Science and Engineering. 2018;454:012132.
27. Hayawi MK, Kareem MM, Ahmed LM. SYNTHESIS OF SPINEL Mn3O4 AND SPINEL Mn_3O_4/ZrO_2 NANOCOMPOSITES AND USING THEM IN PHOTO-CATALYTIC DECOLORIZATION OF Fe(II)-(4,5- DIAZAFLUOREN-9-ONE 11) COMPLEX. Periódico Tchê Química. 2020;17(34):689-699.
28. Ridha NJ, Mohamad Alosfur FK, Kadhim HBA, Ahmed LM. Synthesis of Ag decorated TiO_2 nanoneedles for photocatalytic degradation of methylene blue dye.

Materials Research Express. 2021;8(12):125013.
29. Naseri MG, Saion EB, Ahangar HA, Hashim M, Shaari AH. Simple preparation and characterization of nickel ferrite nanocrystals by a thermal treatment method. Powder Technol. 2011;212(1):80-88.
30. Aliahmad, Noori, Hatefi K, Sargazi. Synthesis of nickel ferrite nanoparticles by co-precipitation chemical method. International Journal of Physical Sciences. 2013;8(18):854-858.
31. Halbus AF, Hussein FH. Photocatalytic Decolorization of Cobalamin in Aqueous Suspensions of TiO_2 and ZnO Under Solar Irradiation. Asian J Chem. 2014;26(4):1207-1211.
32. Ahmed LM, Ivanova I, Hussein FH, Bahnemann DW. Role of Platinum Deposited on TiO_2 in Photocatalytic Methanol Oxidation and Dehydrogenation Reactions. International Journal of Photoenergy. 2014;2014:1-9.
33. Jassim S, Abbas A, Al-Shakban M, Ahmed L. Chemical Vapour Deposition of CdS Thin Films at Low Temperatures from Cadmium Ethyl Xanthate. Egyptian Journal of Chemistry. 2021;64(5):3-4.
34. Ahmed L, Ali S, Ali M. Hybrid Phosphotungstic acid -Dopamine (PTA-DA) Like-flower Nanostructure Synthesis as a Furosemide Drug Delivery System and Kinetic Study of Drug Releasing. Egyptian Journal of Chemistry. 2021;0(0):0-0.
35. Ahmed L, Alkhafaji E, Oda N. Characterization of silver nanohybrid with layers double hydroxide and demonstration inhibition of antibiotic-resistance Staphylococcus aureus. Egyptian Journal of Chemistry. 2022;0(0):0-0.
36. Raees A, Jamal MA, Ahmed I, Silanpaa M, Saad Algarni T. Synthesis and Characterization of CeO_2/CuO Nanocomposites for Photocatalytic Degradation of Methylene Blue in Visible Light. Coatings. 2021;11(3):305.
37. Kooti M, Sedeh AN. Synthesis and Characterization of $NiFe_2O_4$ Magnetic Nanoparticles by Combustion Method. Journal of Materials Science & Technology. 2013;29(1):34-38.
38. Abed z, Mohammad R, Elttayef A. Structural properties of Ag-CuO thin films on silicon prepared via DC magnetron sputtering. Egyptian Journal of Chemistry. 2021;0(0):0-0.
39. Ghosh D, Biswas R. Theoretical Calculation of Absolute Radii of Atoms and Ions. Part 2. The Ionic Radii. Int J Mol Sci. 2003;4(6):379-407.
40. Karaagac O, Atmaca S, Kockar H. A Facile Method to Synthesize Nickel Ferrite Nanoparticles: Parameter Effect. Journal of Superconductivity and Novel Magnetism. 2016;30(8):2359-2369.
41. Talebi R. Preparation of nickel ferrite nanoparticles via a new route and study of their photocatalytic properties. Journal of Materials Science: Materials in Electronics. 2016;28(5):4058-4063.
42. Koli PB, Kapadnis KH, Deshpande UG. Nanocrystalline-modified nickel ferrite films: an effective sensor for industrial and environmental gas pollutant detection. Journal of Nanostructure in Chemistry. 2019;9(2):95-110.
43. Alijani HQ, Iravani S, Pourseyedi S, Torkzadeh-Mahani M, Barani M, Khatami M. Biosynthesis of spinel nickel ferrite nanowhiskers and their biomedical applications. Sci Rep. 2021;11(1).
44. Parveen S, Premkumar T, Poornima S, Govindarajan S. Catalytic activity of nanocrystalline ZnM_2O_4 (M = Fe, Co) prepared via simple and facile synthesis of thermal decomposition of mixed metal complexes of Schiff bases generated from α-ketobutyric acid and diaminoguanidine. Journal of Saudi Chemical Society. 2019;23(6):691-701.
45. Jeseentharani V, George M, Jeyaraj B, Dayalan A, Nagaraja KS. Synthesis of metal ferrite (MFe_2O_4, M = Co, Cu, Mg, Ni, Zn) nanoparticles as humidity sensor materials. J Exp Nanosci. 2013;8(3):358-370.
46. Habibi MH, Fakhri F. Low temperature preparation, characterization, magnetic measurements, thermal, optical, morphological and photo-catalytic properties of nano-size single phase nickel ferrite $NiFe_2O_4$. Journal of Materials Science: Materials in Electronics. 2017;28(18):13455-13463.
47. Goodarz Naseri M, Saion EB, Abbastabar Ahangar H, Shaari AH, Hashim M. Simple Synthesis and Characterization of Cobalt Ferrite Nanoparticles by a Thermal Treatment Method. Journal of Nanomaterials. 2010;2010:1-8.
48. Ezzayani K, Ben Khelifa A, Saint-Aman E, Loiseau F, Nasri H. Complex of hexamethylenetetramine with magnesium-tetraphenylporphyrin: Synthesis, structure, spectroscopic characterizations and electrochemical properties. J Mol Struct. 2017;1137:412-418.
49. Fakhri FH, Ahmed LM. Incorporation CdS with ZnS as Composite and Using in Photo-Decolorization of Congo Red Dye. Indonesian Journal of Chemistry. 2019;19(4):936.
50. Jawad TM, Ahmed LM. DIRECT ULTRASONIC SYNTHESIS OF WO_3/TiO_2 NANOCOMPOSITES AND APPLYING THEM IN THE PHOTODECOLORIZATION OF EOSIN YELLOW DYE. Periódico Tchê Química. 2020;17(34):621-633.
51. Obaid A, Ahmed L. One-Step Hydrothermal Synthesis of α-MoO_3 Nano-belts with Ultrasonic Assist for incorporating TiO2 as a NanoComposite. Egyptian Journal of Chemistry. 2021;0(0):0-0.
52. Jawad TM, Ahmed LM. Synthesis of WO_3/TiO_2 nanocomposites for Use as Photocatalysts for Eosin Yellow Dye Degradation. IOP Conference Series: Materials Science and Engineering. 2021;1067(1):012153.
53. Sharifi S, Yazdani A, Rahimi K. Incremental substitution of Ni with Mn in $NiFe_2O_4$ to largely enhance its supercapacitance properties. Sci Rep. 2020;10(1).
54. Meinert M, Reiss G. Electronic structure and optical band gap determination of $NiFe_2O_4$. J Phys: Condens Matter. 2014;26(11):115503.
55. Nandapure AI, Kondawar SB, Nandapure BI, Choudhari MM. Structural and optical properties of polyaniline/nickel ferrite nanocomposites. Advanced Materials Proceedings. 2021;2(7):463-467.
56. Findik S. Decolorization of Direct Black 22 by Photo Fenton like Method Using UV Light and Zeolite Modified Zinc Ferrite: Kinetics and Thermodynamics. Acta Chimica Slovenica. 2022;69(3):552-563.
57. Prabha I, Lathasree S. Photocatalytic Degradation of Reactive Red 198 Dye Using Zinc Oxide and Titanium Dioxide Nanocatalysts. Asian J Chem. 2014;26(9):2797-2801.
58. Ahmed LM. Photo-Decolourization Kinetics of Acid Red 87 Dye in ZnO Suspension Under Different Types of UV-A Light. Asian J Chem. 2018;30(9):2134-2140.
59. Kzar KO, Mohammed ZF, Saeed SI, Ahmed LM, Kareem DI, Hadyi H, et al. Heterogeneous photo-decolourization of cobaltous phthalocyaninate dye (reactive green dye) catalyzed by ZnO. THE 7TH INTERNATIONAL CONFERENCE ON APPLIED SCIENCE AND TECHNOLOGY (ICAST 2019): AIP Publishing; 2019.

60. Khudhair Abbas S, Hassan ZM, Ahmed LM. Influencing the Artificial UV-A light on decolorization of Chlorazol black BH Dye via using bulk ZnO Suspensions. Journal of Physics: Conference Series. 2019;1294(5):052050.
61. FFECT OF CONCENTRATION ON MICROSTRUCTURAL AND OPTICAL PROPERTIES OF Mn DOPED ZnS NANOPARTICLES BY CHEMICAL CO-PRECIPITATION METHOD. Journal of Xidian University. 2020;14(10).
62. Ahmed LM, Saaed SI, Marhoon AA. Effect of Oxidation Agents on Photo-Decolorization of Vitamin B₁₂ in the Presence of ZnO/UV-A System. Indonesian Journal of Chemistry. 2018;18(2):272.
63. Jasim KM, Ahmed LM. TiO_2 Nanoparticles Sensitized by Safranine O Dye using UV-A Light System. IOP Conference Series: Materials Science and Engineering. 2019;571(1):012064.
64. Bousalah D, Yeddou AR, Hachemi M, Chergui A, Nadjemi B. OXIDATION OF AZO DYE CARMOISINE (E122) IN AQUEOUS SOLUTION BY HETEROGENEOUS CATALYST CuO/Al2O3 SYSTEM. Environmental Engineering and Management Journal. 2021;20(2):167-175.
65. Construction of Green Credit System for Commercial Banks. International Journal of Science and Research (IJSR). 2017;6(7):506-510.
66. Sekar A, Yadav R. Green fabrication of zinc oxide supported carbon dots for visible light-responsive photocatalytic decolourization of Malachite Green dye: Optimization and kinetic studies. Optik. 2021;242:167311.